Observer based direct control strategy for a multi-level three phase flying-capacitor inverter

Saber Laamiri, Malek Ghanes, Gaetan Santomenna

Version of Record: https://www.sciencedirect.com/science/article/pii/S0967066119300322
Manuscript_238f4db44588ff5ef8d084bf76653014

Observer based Direct Control Strategy for a Multi-Level Three Phase Flying-Capacitor Inverter

S. Laamiri[a,b], M. Ghanes[a], G. Santomenna[b]

[a]*Ecole Centrale de Nantes, LS2N, CNRS, 1 rue de la Noë, 44321 Nantes Cedex 3, France*
(saber.laamiri@ec-nantes.fr, malek.ghanes@ec-nantes.fr)
[b]*GS Maintenance Company, 184 rue Pascal, 77000, Vaux Le Pénil, France (gaëtansantomenna@yahoo.fr, gsm77@gsmaintenance.fr)*

Abstract

Thanks to the series of connections taking place in commutation cells, flying-capacitor converters provide a means of increasing power and voltage, better harmonic content with reduced dv/dt and can be reconfigured in order to work in degraded mode. However, all these advantages come to the price of a more complex structure, which leads to more complex control strategies. On the other hand, capacitor voltages sensors which are usually expensive, bulky and can degrade the system's reliability, especially in a hostile environment. To overcome both problems (control complexity and capacitor voltages measurements) and motivated by an industrial application with GS Maintenance company, a simple control strategy and an adaptive observer, scalable to any number of cells, are designed for a multi-level DC bus midpoint three-phase FCI (Flying-Capacitor Inverter). Furthermore, the stability of the proposed control strategy and observer design is proved by means of Lyapunov theory. Finally, the good performance under load resistance, cells capacitor and input variations through experimental results is showed in case of a DC bus midpoint 3-cells 4-levels three phase FCI.

Keywords: Multilevel flying capacitor inverter, Direct control strategy, Observer design, Lyapunov stability, Robustness, Texas instruments DSP, Xilinx FPGA.

1. Introduction

High power levels are needed in many industrial applications: active filters, motor drives, HVDC (High-Voltage Direct Current) transmission, FACTS (Flexible Alternating Current Transmission System) Lezana et al. (2008), Meynard et al. (2002). In such applications voltage stress of power electronic switches should be avoided. In Sweden HVDC Light transmission system, March 1997, such phenomena is reduced by connecting in series power electronic switches Eriksson et al. (1998). However, voltage balancing among devices at steady and transient states is the main problem arising beyond this technique Van Nguyen et al. (2010). Thereby, the use of multi-level FCI introduced by Meynard and Foch in 1992 Meynard and Foch (1992) appears as a natural solution. As it is composed of a series of elementary commutation cells, linked with floating voltage sources, it can be used in high voltage with minimum voltage stress on switching devices (high voltages distribution over more switching elements) and generate an output voltage with reduced harmonic content. Moreover, it offers low voltage jump (dv/dt), which results in reduced stress on motor bearing in drive applications Ghanes et al. (2016), Stala et al. (2009). Also, its output frequency is multiplied by its cell number, which allows reducing the filtering elements.

However, the constraint of this type of converter is that the presence of flying capacitors requires balancing their voltages. To solve the problem of voltage capacitors balancing, several methods are presented in literature with different control laws: open loop controllers that guarantee a natural balancing Shukla et al. (2011), Thielemans et al. (2010) and closed loop controllers that can improve balancing dynamics Ben Said et al. (2014), Brychcín et al. (2016).

Motivated by an industrial application with GS Maintenance company, the first contribution of this work is to extend the simple direct control law combining the projection strategy with a classical sliding mode technique, proposed in Laamiri et al. (2017), for a multi-level DC bus midpoint three-phase FCI scalable to any number of cells. To the best knowledge of the authors, this type of control is not yet designed for this topology.

On the other hand, whenever the number of levels increases, multi-level FCI needs a large number of capacitors and more voltage sensors which increase the cost and the complexity of the system. Thus, the estimation of the capacitor voltages by an observer has become an attractive solution and is less expensive. Many types of observers for multi-level converters are proposed such as finite-time observers Defoort et al. (2011), Benzineb et al. (2013) and adaptive observers Ghanes et al. (2014), Ghanes et al. (2016).

Motivated again by an industrial application with GS Maintenance company, the second contribution of this work is to propose an adaptive observer to estimate capacitor voltages of a multi-level DC bus midpoint three phase FCI scalable to any number of cells by using only current sensors. To the best knowledge of the authors, the dedicated observer has not yet been considered in the literature for the proposed inverter topology.

Furthermore, stability analysis of the proposed control strategy, of the dedicated observer and of the observer based control strategy are given by using Lyapunov theory.

Finally, the proposed observer based control strategy has been implemented in a real-time against an experimental set-up in case of a DC bus midpoint 3-cells 4-levels three phase FCI. To show the applicability of the proposed methodology when the number of cells increases, simulation results are presented in case of a 7-cells 8-levels FCI (the experimental set-up of this case is in progress at GS Maintenance company and is confidential).

This paper is organized as follows. In section 2, a modeling of the DC source midpoint multi-level three phase FCI and its characteristics are presented. The proposed control strategy is presented in section 3 while section 4 details the design of the dedicated observer for the considered inverter topology. Based on Lyapunov theory the stability analysis of the observer based control strategy is given in section 5. Section 6 presents, through experimental tests, the performances (tracking and robustness) of the proposed control and observer methodology in case of a DC bus midpoint 3-cells 4-levels three phase FCI and shows simulation results in case of a 7-cells 8-levels FCI. The paper ends with a conclusion in section 7.

2. DC source midpoint multi-level three phase FCI modeling

2.1. Operating principle

The presented three phase multi-cell multi-level FCI with a DC source midpoint is illustrated in Figure 1.

The system under study consists of p-cells, separated by $p-1$ capacitors for each leg. The series connection between these cells, linked by capacitors, and a RL load can be considered as continuous sources Al-Hammouri et al. (2012), Sadigh et al. (2010).

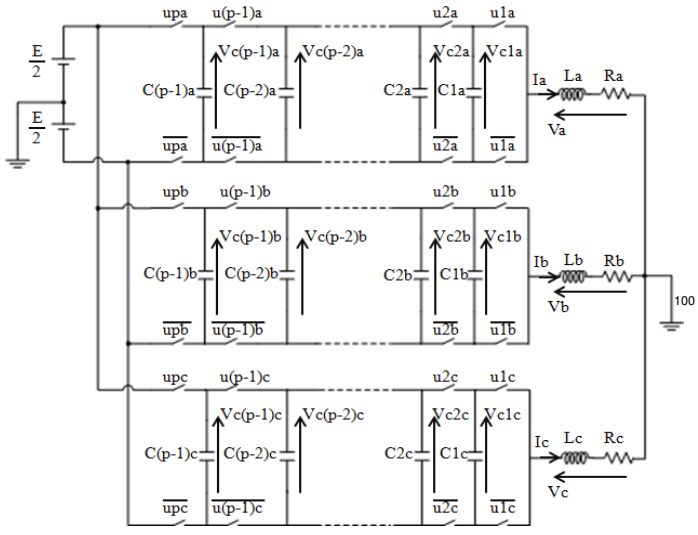

Figure 1: Three phase p-cells inverter connected to a RL load

Each cell contains two complementary power electronic components controlled by a binary (discrete) switch u_k, k=[1, 2, ..., p]. u_k=1 (respectively u_k=0) when the upper switch (respectively lower switch) in $cell_k$ is conducting. It is a hybrid system where both continuous (floating capacitor voltages) and discrete (binary switches) variables evolve.

In order to ensure normal operations, it is necessary to guarantee a balanced distribution of the capacitor voltages as following Béthoux et al. (2008), Aguilera et al. (2015).

$$V_{ck} = k\frac{E}{p} \tag{1}$$

where E is the DC source.

Each cell k is located between two floating capacitor voltages, so

$$V_{cellk} = V_{ck} - V_{ck-1} \tag{2}$$

where $V_{c0} = 0$ and $V_{cp} = E$.

Cell voltages take the same value under equilibrium conditions. Therefore

$$V_{cellk} = \frac{E}{p}. \tag{3}$$

Consequently, electrical stresses on each switch are reduced and more equally distributed as each switch must withstand $\frac{E}{p}$ volts Aguilera et al. (2015), Hosseini et al. (2009).

Depending on the configuration of switches, output voltages have p+1 levels: $[\frac{-E}{2}, (\frac{-E}{2}+\frac{E}{p}), ..., (\frac{E}{2}-\frac{E}{p}), \frac{E}{2}]$, which means that dv/dt decreases compared to classical structures of converters.

2.2. Modeling

Each leg of multi-level FCI with a DC source midpoint can be represented by p differential equations (4)

$$\begin{cases} \frac{dV_{ckj}}{dt} = \frac{1}{C_{kj}}\Delta u_{kj} i_j \\ \frac{di_j}{dt} = -\sum_{k=1}^{p-1}\Delta u_{kj}\frac{V_{ckj}}{L_j} - \frac{R_j}{L_j}i_j + (u_{pj} - \frac{1}{2})\frac{E}{L_j} \end{cases} \tag{4}$$

where j refers to legs a, b or c, $k = 1, ..., p-1$ represents the number of capacitor voltages, V_{ckj} is the capacitor voltage of leg j, C_{kj} denotes the capacitor k of leg j and i_j is the output current of leg j.

The binary (discrete) switch k of leg j is represented by u_{kj} and the current path is defined as

$$\Delta u_{kj} = u_{(k+1)j} - u_{kj}. \tag{5}$$

R_j and L_j are the load resistance and load inductance of leg j, respectively.

The state space representation is given by

$$\begin{cases} \dot{X}_j = A_j(\Delta u)X_j + B_j(u_{pj}, E) + D_j(E) \\ y = CX_j \end{cases} \tag{6}$$

where $\Delta u = [\Delta u_{1j}, ..., \Delta u_{(p-1)j}]$, $\Delta u \in \{-1, 0, 1\}^{1\times(p-1)}$, $X_j = \begin{bmatrix} V_{c1j} & ... & V_{c(p-1)j} & i_j \end{bmatrix}^T$,

$$A_j(\Delta u) = \begin{bmatrix} 0 & ... & 0 & \frac{\Delta u_{1j}}{C_{1j}} \\ \vdots & \vdots & \vdots & \vdots \\ 0 & ... & 0 & \frac{\Delta u_{(p-1)j}}{C_{(p-1)j}} \\ -\frac{\Delta u_{1j}}{L_j} & ... & -\frac{\Delta u_{(p-1)j}}{L_j} & -\frac{R_j}{L_j} \end{bmatrix},$$

$C = \begin{bmatrix} 0 & ... & 0 & 1 \end{bmatrix}$, $B_j(u_{pj}, E) = \begin{bmatrix} 0 & ... & 0 & \frac{u_{pj}}{L_j}E \end{bmatrix}^T$ and $D_j(E) = \begin{bmatrix} 0 & ... & 0 & -\frac{E}{2L_j} \end{bmatrix}^T$.

An average model of the inverter Benzineb et al. (2011), in which all the signals are continuous, can be defined as follows

$$\begin{cases} \frac{dV_{ckj}}{dt} = \frac{1}{C_{kj}}\Delta\alpha_{kj} i_j \\ \\ \frac{di_j}{dt} = -\sum_{k=1}^{p-1} \Delta\alpha_{kj}\frac{V_{ckj}}{L_j} - \frac{R_j}{L_j} i_j + (\alpha_{pj} - \frac{1}{2})\frac{E}{L_j} \end{cases} \quad (7)$$

where the switching controls Δu_{kj} are replaced by their average values (duty cycles) along the sample period, i.e. $\Delta\alpha_{kj} = \frac{1}{T_s}\int_0^{T_s} \Delta u_{kj} dt$, with $\Delta\alpha_{kj} = \alpha_{(k+1)j} - \alpha_{kj}$.

3. Control strategy

3.1. Principle

As it was mentioned in the introduction, the capacitor voltages control objective of the DC source midpoint multi-level three phase FCI is relevant. In this part a direct control strategy, which is scalable and easy to implement is proposed to achieve the objective. The idea is to find a switching state u_k (control) for each leg j of the inverter in order to bring to zero fast as possible the error between the measured capacitors voltages and the reference (desired) ones, defined as follows

$$\Delta V_{ckj} = V_{ckj} - V_{ckj-ref}. \quad (8)$$

Assumption 1. *The capacitor reference $V_{ckj-ref}$ is considered constant.*

Defining λ as the number of upper switches turned ON.
If $\lambda = 0$, the output voltage V_j takes the value $-\frac{E}{2}$.
If $\lambda = p$, the output voltage V_j takes the value $\frac{E}{2}$.
If $\lambda \neq 0$ and $\lambda \neq p$, for each leg, a strategy of control is proposed, which consists of computing ΔV_{ck}, defined in (8), on each one of the $p-1$ possibles evolution of the capacitor voltages dynamics $\dot{V}_{ckj}$ and picking the largest one for each leg j given by (9).
This proposed control strategy can be written in a formal way as follows

$$u_{bestj} = \{\left(u_{(p-1)j}, ..., u_{1j}\right) / \max\{\Delta V_{ckj}.\dot{V}_{ckj}\}\} \quad (9)$$

where u_{bestj} is the largest projection, which corresponds to a sequence of control $\left(u_{(p-1)j}, ..., u_{1j}\right)$, where u_k is defined in subsection 2.1. It is used on the current path (5) and applied to the power components of the inverter (see Figure 1) in order to control the capacitor voltages.
By replacing in (9) the dynamics $\dot{V}_{ckj}$ by its expression given in (4), the control strategy (9) can be rewritten as

$$u_{bestj} = \{\left(u_{(p-1)j}, ..., u_{1j}\right) / \{\max(\Delta V_{ckj}.\Delta u_{kj}) sign(i_j)\} \quad (10)$$

which allows to simplify the computation for each leg of the inverter.

3.2. Implementation issues

As it can be seen from the proposed control strategy (10) that only the sign of the current for each leg of the inverter i_j is needed (exact value of i_j is not necessary).
In other terms, only the current direction i_j is needed, which simplifies the sensing circuitry that can be reduced to a single comparator. Another advantage in doing so is to reduce the cost of using an analog to digital converter (ADC) in digital systems, which is an expensive resource. A simple digital input indicating whether the current is positive or negative makes the job. In terms of capacitor voltages, the accuracy of measurement is not needed because a margin of error is tolerated on the capacitor voltages. The objective of the proposed observer based control (see next sections) is to assign the voltage output of the inverter to its reference and to keep the capacitor voltages on the fixed margins. Table 1 presents the evolution of capacitor voltages (charging, discharging or floating) under the action of the proposed strategy with the aim to show its simplicity, where $u_j = [u_{pj}, u_{(p-1)j}, \ldots, u_{2j}, u_{1j}]$ is the state switching vector for leg j. The state switching applied for voltage capacitors balancing u_{bestj} is what assures the maximum scalar product with ΔV_{cj}.

uj	Vc(p-1)j	Vc(p-2)j	⋯⋯	Vc2j	Vc1j
[0,0,..,0,1]	~	~	~	~	↘
[0,0,..,1,0]	~	~	~	↘	↗
⋮	⋮	⋰	⋰	⋰	~
⋮	~	⋰	⋰	⋰	⋮
[0,1,..,0,0]	↘	↗	~	~	~
[1,0,..,0,0]	↗	~	~	~	~

Table 1: Capacitor voltages evolution in the p-cells inverter with positive load current i_j and $\lambda = 1$

3.3. Stability analysis

The control strategy described in subsection 3.1 allows to choose the current path Δu_{kj}, defined in (5), as follows

$$\Delta u_{kj} = -sign(i_j) sign(\Delta V_{ckj}) \quad (11)$$

which corresponds to have λ, the number of upper switches tuned ON different from 0 and p, i.e. $\lambda = 1, ..., p-1$.
In the case where $\Delta u_{kj} = 0, k = 1, ..., p-1$, occurs in an interval of time $[t_i; t_{i+1}[$, which corresponds to have λ equal to 0 or 1, all capacitors of the inverter are bypassed.
By using assumption 1, the dynamics of (8) is given by

$$\Delta\dot{V}_{ckj} = \Delta u_{kj}\frac{i_j}{C_{kj}} \quad (12)$$

where the current path Δu_{kj} used in the first equation of (4) is replaced by (11).

Lemma 3.1. *Let assumption 1 hold. Then, the capacitor voltages error dynamics (12) of the inverter with the proposed control strategy (10)-(11), has an asymptotic stability if the current path Δu_{kj} and the output current i_j are different from zero.*

When Δu_{kj} or i_j is equal to zero, the capacitor voltages error dynamics (12) is Lyapunov stable.

Proof 3.2. *To prove the stability of the proposed control strategy, let be V_{ctrl} a Lyapunov candidate function*

$$V_{ctrl} = \sum_{k=1}^{p-1} \frac{1}{2} {\Delta V_{ckj}}^2 \tag{13}$$

The first derivative of (13) *along trajectories of* (12) *(where* (11) *is replaced) is given by*

$$\begin{aligned} \dot{V}_{ctrl} &= -\sum_{k=1}^{p-1} \Delta V_{ckj} sign(\Delta V_{ckj}) sign(i_j) \frac{i_j}{C_{kj}} \\ &= -\sum_{k=1}^{p-1} |\Delta V_{ckj}| \frac{|i_j|}{C_{kj}} < 0 \end{aligned} \tag{14}$$

where $V_{ckj-ref}$ is considered constant.
Consequently, the asymptotic stability of (12) *is ensured by the proposed strategy when Δu_{kj} and i_j are different from zero. According to Poznyak et al. (2011), this is a sufficient condition for finite-time convergence.*
However, when the current path (resp. the output current) is equal to zero ($\Delta u_{kj} = 0$ (resp. $i_j = 0$)), the Lyapunov function defined in (13) *is constant ($\dot{V} = 0$), which means that there is no evolution of the capacitor voltages, i.e. no current passes through the capacitors (all capacitors are bypassed). Consequently, only a Lyapunov stability of the dynamics error* (12) *is ensured.*

Remark 1. If assumption 1 is not satisfied (DC bus voltage of the inverter presents some fluctuations), the condition of stability in (14) becomes as follows

$$\dot{V}_{ctrl} \leq -\sum_{k=1}^{p-1} |\Delta V_{ckj}| \left(\frac{|i_j|}{C_{kj}} - |\dot{V}_{ckj-ref}| \right),$$

which implies that

$$|\dot{V}_{ckj-ref}| < \frac{|i_j|}{C_{kj}}. \tag{15}$$

In practice, inequality (15) is almost satisfied because the variation of $V_{ckj-ref}$ is close to zero except for the special cases such as spikes or sudden failures of the DC bus voltage. In the present work, this variation (perturbation) is due to power switches elements (quality of the snubber) and it is function of the current load amplitude. As is shown for example in figure 5, no perturbation appears when the current load is equal to zero, therefore condition (15) is verified. Moreover, the capacitors C_{kj} are sized to cancel the effect of this sudden variation.

4. Observer

In this section, the observer design for the proposed DC bus midpoint multi-level three phase FCI modeled by (6) is presented by taking into account the observability study described in the following subsection. The observability study and the observer design are presented and analyzed based on instantaneous model ((4) and (16)) whereas switching control law u_k is introduced by mean of state (0 or 1).

4.1. Observability study and new modeling

Observability study.
This study aims to characterize the observability of the capacitor voltages V_{ckj}, using the measured output current i_j (and its derivatives) and the grid voltage E. For that, the dynamic equation of the output current given in (4) is considered.
Then, $p-1$ distinct cases can be observed from current path (5).
- During switching time t_1: $\Delta u = [\Delta u_{1j}, ..., \Delta u_{(p-1)j}] = [1, 0, ..., 0]$: V_{c1j} is observable and $\dot{V}_{ckj} = 0$ for $k = 2, ..., p-2$ (V_{ckj} are not observables).
- During switching time t_2: $\Delta u = [\Delta u_{1j}, ..., \Delta u_{(p-1-j}] = [0, 1, 0, ..., 0]$: V_{c2j} is observable and $\dot{V}_{ckj} = 0$, $k = 1, ..., p-1$, $k \neq 2$ (V_{ckj} are not observables).
- During switching time t_k: $\Delta u = [\Delta u_{1j}, ..., \Delta u_{(p-1)j}] = [0, ..., 0, 1]$: $V_{c(p-1)j}$ is observable and $\dot{V}_{ckj} = 0$, $j = 1, ..., p-2$ (V_{ckj} are not observables).

Definition 4.1. *A specific switching sequence (see also Kang et al. (2009), Ghanes et al. (2014)) is defined when T_c is large enough to contain at least the $p-1$ configurations $\Delta u = [1, 0, ..., 0]$, ..., $\Delta u = [0, 0, ..., p-1]$. The switching state $\tilde{sw}$ associated to $[t - T_c, t]$ is called a switching sequence (see also Lygeros et al. (2003)) where T_c is a cycle of time.*

Then if for any t there are t_1, t_2, ..., t_{p-1} in $[t - T_c, t]$ such that $rank \begin{pmatrix} \Delta u_{1j}(t_1) & ... & \Delta u_{(p-1)j}(t_1) \\ \Delta u_{1j}(t_2) & ... & \Delta u_{(p-1)j}(t_2) \\ \vdots & ... & \vdots \\ \Delta u_{1j}(t_k) & ... & \Delta u_{(p-1)j}(t_k) \end{pmatrix} = p-1$, then V_{c1j}, ..., $V_{c(p-1)j}$ are observables.
With respect to observability study of DC bus midpoint multilevel three phase FCI, the objective is to split the model (6) into a $(p-1)$-subsystems in order to make the observer design possible, to estimate the capacitor voltages V_{ckj}, ..., $V_{c(p-1)j}$. In doing so, a set of observers will be designed for the whole system, from the separate synthesis of set observers for each subsystem.

New modeling.
With this aim in view, the DC bus midpoint multi-level three phase FCI model (6) can be rewritten in the following coupled $(p-1)$-subsystems of the form

$$\Sigma : \begin{cases} \dot{X}_{1j} &= A_{1j}(\Delta u_{1j}) X_{1j} + B_j(\Delta u, y) + D_j(y) \\ & \quad + W_{1j}(\Delta u, X) \\ \dot{X}_{2j} &= A_{2j}(\Delta u_{2j}) X_{2j} + B_j(\Delta u, y) + D_2(y) \\ & \quad + W_{2j}(\Delta u, X) \\ \vdots & \\ \dot{X}_{(p-1)j} &= A_{(p-1)j}(\Delta u_{(p-1)j}) X_{(p-1)j} + B_j(\Delta u, y) \\ & \quad + D_j(y) + W_{(p-1)j}(\Delta u, X) \\ y &= \bar{C} X_{kj} \end{cases} \tag{16}$$

with $X_{kj} = \begin{bmatrix} i_j \\ V_{ckj} \end{bmatrix}$, $A_{kj}(\Delta u_{kj}) = \begin{bmatrix} -\frac{R_j}{L_j} & -\frac{\Delta u_{kj}}{L_j} \\ \frac{\Delta u_{kj}}{C_{kj}} & 0 \end{bmatrix}$, $k = 1, ..., p-1$,

$W_{\eta j}(\Delta u, X) = -\frac{1}{L_j}\begin{bmatrix} \sum_{k=1,k\neq\eta}^{p-1} \Delta u_{kj} V_{ckj} & 0 \end{bmatrix}^T$, $\eta = 1, ..., p-1$,

$B_j(\Delta u, y) = \begin{bmatrix} \frac{E}{L_j} u_{pj} \\ 0 \end{bmatrix}$, $D_j(y) = \begin{bmatrix} -\frac{E}{2L_j} \\ 0 \end{bmatrix}$, $\bar{C} = \begin{bmatrix} 1 & 0 \end{bmatrix}^T$.

The studied observability (4.1) means that the capacitors C_{kj} should be crossed by the current flow (5) for a time that would be long enough. These two conditions are respectively ensured by the following assumptions.

Assumption 2.
1. The $p-1$ configurations of switches $\Delta u = [1, 0, ..., 0]$, ..., $\Delta u = [0, 0, ..., p-1]$ are applied at least one time.
2. Considering t_i, the switching instants between two configurations of switches among the p ones defined in (5) *and τ_{min} the dwell time. Then, there exists a constant $\tau_{min} > 0$ such that the length $(t_{i+1} - t_i)$ of any interval of time $[t_i; t_{i+1}[$ is greater than τ_{min}.*

Property 1.
$W_{\eta j}(\Delta u, X)$ is Lipschitz w.r.t X and uniformly w.r.t. Δu.

4.2. Observer design

By taking into account the observability study described in subsection (4.1) and based on model (16), the observer design is presented for the studied DC bus midpoint multi-level three phase FCI

$$
O: \begin{cases}
\dot{\hat{X}}_{1j} &= A_{1j}(\Delta u_{1j})\hat{X}_{1j} + B_j(\Delta u, y) + W_{1j}(\Delta u, \hat{X}) \\
&\quad + D_j(y) + g u_{1j} \Xi_{1j}^{-1} \bar{C}^T (y - \hat{y}) \\
\dot{\Xi}_{1j} &= -\zeta_{1j}\Xi_{1j} \\
&\quad + u_{1j}\left[-A_{1j}^T(\Delta u_{1j})\Xi_{1j} - \Xi_{1j}^i A_{1j}(\Delta u_{1j})\right] \\
&\quad + 2g u_{1j} \bar{C}^T \bar{C} \\
\dot{\hat{X}}_{2j} &= A_{2j}(\Delta u_{2j})\hat{X}_{2j} + B_j(\Delta u, y) + W_{2j}(\Delta u, \hat{X}) \\
&\quad + D_j(y) + g u_{2j} \Xi_{2j}^{-1} \bar{C}^T (y - \hat{y}) \\
\dot{\Xi}_{2j} &= -\zeta_{2j}\Xi_{2j} \\
&\quad + u_{2j}\left[-A_{2j}^T(\Delta u_{2j})\Xi_{2j} - \Xi_{2j} A_{2j}(\Delta u_{2j})\right] \\
&\quad + 2g u_{2j} \bar{C}^T \bar{C} \\
&\vdots \\
\dot{\hat{X}}_{p-1} &= A_{(p-1)j}(\Delta u_{(p-1)j})\hat{X}_{(p-1)j} + B_j(\Delta u, y) \\
&\quad + W_{(p-1)j}(\Delta u, \hat{X}) + D_j(y) \\
&\quad + g u_{p-1} \Xi_{(p-1)j}^{-1} \bar{C}^T (y - \hat{y}) \\
\dot{\Xi}_{(p-1)j} &= -\zeta_{(p-1)j}\Xi_{(p-1)j} \\
&\quad - u_{(p-1)j}\left[A_{(p-1)j}^T(\Delta u_{(p-1)j})\Xi_{(p-1)j}\right] \\
&\quad - u_{(p-1)j}\left[\Xi_{(p-1)j} A_{(p-1)j}(\Delta u_{(p-1)j})\right] \\
&\quad + 2g u_{(p-1)j} \bar{C}^T \bar{C} \\
\hat{y} &= \bar{C}\hat{X}_{kj}, k = 1, ..., p-1,
\end{cases}
\tag{17}
$$

where $\hat{X}_{kj} = \begin{bmatrix} \hat{I} \\ \hat{V}_{ckj} \end{bmatrix}$,

$W_{\eta j}(\Delta u, \hat{X}) = -\frac{1}{L_j}\begin{bmatrix} \sum_{k=1,\eta\neq k}^{p-1} \Delta u_{kj} \hat{V}_{ckj} & 0 \end{bmatrix}^T$, $\eta = 1, ..., p-1$,

$g u_{\eta j} = |u_{\eta j}|\left[\prod_{k=1,\eta\neq k}^{p-1}(1 - |u_{kj}|)\right]$, $\zeta_{1j} > 0, ..., \zeta_{(p-1)j} > 0$ and $\Xi_{1j}^{-1}\bar{C}^T, ..., \Xi_{(p-1)j}^{-1}\bar{C}^T$ are the gains of the observer. $\Xi_{1j}, \ldots, \Xi_{(p-1)j}$ are symmetric positive definite matrices and bounded away from zero (see Ghanes et al. (2014) for more details in case of $p = 3$ (3 cells) and $j = a$ (chopper)). To prove the convergence of the proposed observer, the estimation error between system (16) and observer (17) is considered

$$
\begin{cases}
e_{1j} &= X_1 - \hat{X}_1 \\
e_{2j} &= X_2 - \hat{X}_2 \\
&\vdots \\
e_{(p-1)j} &= X_{p-1} - \hat{X}_{p-1}
\end{cases}
\tag{18}
$$

whose dynamics is

$$
\begin{cases}
\dot{e}_{1j} &= \left(A_{1j}(\Delta u_{1j}) - g u_{1j}\Xi_{1j}^{-1}\bar{C}^T\bar{C}\right)e_1 \\
&\quad + W_{1j}(\Delta u, X) - W_{1j}(\Delta u, \hat{X}) \\
&\vdots \\
\dot{e}_{(p-1)j} &= \left(A_{(p-1)j}(\Delta u_{(p-1)j}) - g u_{(p-1)j}\Xi_{(p-1)j}^{-1}\bar{C}^T\bar{C}\right) \\
&\quad e_{(p-1)j} + W_{(p-1)j}(\Delta u, X) - W_{(p-1)j}(\Delta u, \hat{X})
\end{cases}
\tag{19}
$$

Theorem 4.2. *Consider system* (16) *and property 1 with assumptions 2-1, 2-2 hold. Then, observer* (17) *is an exponential observer of system* (16) *with large enough tunning gains $\zeta_{kj} > 0$.*

Proof 4.3. *Let V_{obs} be a Lyapunov candidate function*

$$
V_{obs} = \sum_{k=1}^{p-1} e_{kj}^T \Xi_{kj} e_{kj}. \tag{20}
$$

The expression of its dynamics reads as

$$
\begin{cases}
\dot{V}_{obs} &= -\zeta_{1j} e_{1j}^T \Xi_{1j} e_{1j} + (1 \\
&\quad - |u_{1j}|) e_1^T \left[A_{1j}^T(\Delta u_{1j})\Xi_{1j} + \Xi_{1j} A_{1j}(\Delta u_{1j})\right] e_{1j} \\
&\quad + 2 e_{1j}^T \Xi_{1j}\left[W_{1j}(\Delta u, X) - W_{1j}(\Delta u, \hat{X})\right] \\
&\quad + \ldots \\
&\quad - \zeta_{(p-1)j} e_{(p-1)j}^T \Xi_{(p-1)j} e_{(p-1)j} \\
&\quad + (1 \\
&\quad - |u_{(p-1)j}|) e_1^T \left[A_{(p-1)j}^T(\Delta u_{(p-1)j})\Xi_{(p-1)j}\right] e_{(p-1)j} \\
&\quad + (1 \\
&\quad - |u_{(p-1)j}|) e_1^T \left[\Xi_{(p-1)j} A_{(p-1)j}(\Delta u_{(p-1)j})\right] e_{(p-1)j} \\
&\quad + 2 e_{(p-1)j}^T \Xi_{(p-1)j} \\
&\quad \times \left[W_{(p-1)j}(\Delta u, X) - W_{(p-1)j}(\Delta u, \hat{X})\right]
\end{cases}
\tag{21}
$$

From (21)*, two situations can happen.*
Situation 1:
When $\Delta u_{kj} \neq 0$ defined in (11) *(1 or −1) occurs in an interval*

of time $[t_i; t_{i+1}[$*, then the derivative of* V_{obs} (21) *becomes*

$$\left\{\begin{array}{rcl}\dot{V}_{obs} & \leq & -\zeta_{1j}e_{1j}^T\Xi_{1j}e_{1j} + 2\|e_{1j}\|\|\Xi_{1j}\| \\ & & \times\|\left[W_{1j}(\Delta u, X) - W_{1j}(\Delta u, \hat{X})\right]\| \\ & & + \ldots \\ & & -\zeta_{(p-1)j}e_{(p-1)j}^T\Xi_{(p-1)j}e_{(p-1)j} \\ & & +2\|e_{(p-1)j}\|\|\Xi_{(p-1)j}\| \\ & & \times\|\left[W_{(p-1)j}(\Delta u, X) - W_{(p-1)j}(\Delta u, \hat{X})\right]\|\end{array}\right. \quad (22)$$

From property 1 and by using the following inequalities $\underline{\lambda}_{kj}\|e_{kj}\|^2 \leq \|e_{kj}\|^2_{\Xi_{kj}} \leq \overline{\lambda}_{kj}\|e_{kj}\|^2$, $\sqrt{V(e_z)}\sqrt{V(e_y)} \leq \frac{\nu}{2}V(e_z) + \frac{V(e_y)}{2\nu}$, $\forall\, \nu \in]0, 1[$*, where* $\overline{\lambda}_{kj}$ *and* $\underline{\lambda}_{kj}$ *are the largest and smallest eigenvalues of* Ξ_{kj} *respectively.*

$$\left\{\begin{array}{rcl}\dot{V}_{obs} & \leq & -\zeta_{1j}e_{1j}^T\Xi_{1j}e_{1j} + |\Delta u_{2j}|\,\mu_{(1,2)j}\,\nu V_{1j} \\ & & +|\Delta u_{2j}|\,\mu_{(1,2)j}\,\frac{1}{\nu}V_{2j} \\ & & + \ldots + |\Delta u_{(p-1)j}|\,\mu_{(1,(p-1))j}\,\nu V_{1j} \\ & & +|\Delta u_{(p-1)j}|\,\mu_{(1,(p-1))j}\,\frac{1}{\nu}V_{(p-1)j} \\ & & -\zeta_{2j}e_{2j}^T\Xi_{2j}e_{2j} + |\Delta u_{1j}|\,\mu_{(2,1)j}\,\nu V_{2j} \\ & & +|\Delta u_{1j}|\,\mu_{(2,1)j}\,\frac{1}{\nu}V_{1j} \\ & & + \ldots + |\Delta u_{(p-1)j}|\,\mu_{(2,(p-1))j}\,\nu V_{1j} \\ & & +|\Delta u_{(p-1)j}|\,\mu_{(2,(p-1))j}\,\frac{1}{\nu}V_{(p-1)j} \\ & & - \ldots \\ & & \vdots \\ & & -\zeta_{(p-2)j}e_{(p-2)j}^T\Xi_{(p-2)j}e_{(p-2)j} + \ldots \\ & & -\zeta_{(p-1)j}e_{(p-1)j}^T\Xi_{(p-1)j}e_{(p-1)j} \\ & & +|\Delta u_{1j}|\,\mu_{((p-1),1)j}\,\frac{1}{\nu}V_{(p-1)j} \\ & & +|\Delta u_{1j}|\,\mu_{((p-1),1)j}\,\nu V_{1j} \\ & & + \ldots + |\Delta u_{(p-2)j}|\,\mu_{((p-1),(p-2))j}\,\nu V_{(p-1)j} \\ & & +|\Delta u_{(p-2)j}|\,\mu_{((p-1),(p-2))j}\,\frac{1}{\nu}V_{(p-2)j}\end{array}\right. \quad (23)$$

where $\mu_{(1,2)j} = \frac{\|\Xi_{1j}P_r\|}{L\sqrt{\underline{\lambda}_{1j}\underline{\lambda}_{2j}}}$, $\mu_{(2,1)j} = \frac{\|\Xi_{2j}P_r\|}{L\sqrt{\underline{\lambda}_{2j}\underline{\lambda}_{1j}}}$, $\mu_{(1,(p-1))j} = \frac{\|\Xi_{1j}P_r\|}{L\sqrt{\underline{\lambda}_{1j}\underline{\lambda}_{(p-1)j}}}$, $\mu_{(2,(p-1))j} = \frac{\|\Xi_{2j}P_r\|}{L\sqrt{\underline{\lambda}_{2j}\underline{\lambda}_{(p-1)j}}}$, …, $\mu_{((p-1),1)j} = \frac{\|\Xi_{(p-1)j}P_r\|}{L\sqrt{\underline{\lambda}_{(p-1)j}\underline{\lambda}_{1j}}}$, …, $\mu_{((p-1),(p-2))j} = \frac{\|\Xi_{(p-1)j}P_r\|}{L\sqrt{\underline{\lambda}_{(p-1)j}\underline{\lambda}_{(p-2)j}}}$.

Then, by writing (23) *in a compact form in terms of* V_{kj}*, it follows*

$$\left\{\begin{array}{rcl}\dot{V}_{obs} & \leq & -\alpha_j\,\sum_{k=1}^{p-1}V_{kj} = -\alpha_j\,V_{obs}\end{array}\right. \quad (24)$$

where observer gains $\zeta_j = min\{\zeta_{1j}, ..., \zeta_{(p-1)j}\}$ *are selected according to* (25)*.*

$$\left\{\begin{array}{rcl}\alpha_{1j} & = & \zeta_{1j} - \bar{\mu}_{1j} > 0 \\ \vdots & & \\ \alpha_{(p-1)j} & = & \zeta_{(p-1)j} - \bar{\mu}_{(p-1)j} > 0\end{array}\right. \quad (25)$$

with $\bar{\mu}_{1j} = \left(|\Delta u_{2j}|\,\mu_{(1,2)j}\,\nu + ... + |\Delta u_{1j}|\,\mu_{(2,1)j}\,\frac{1}{\nu}\right), \ldots,$ $\bar{\mu}_{(p-1)j} = \left(|\Delta u_{1j}|\,\mu_{((p-1),1)j}\,\frac{1}{\nu} + ... + |\Delta u_{(p-1)j}|\,\mu_{(1,(p-1))j}\,\nu\right)$.

Situation 2:

When $\Delta u_{kj} = 0$*,* $k = 1, ..., p-1$ *(all capacitors are bypassed) occurs in an interval of time* $[t_i; t_{i+1}[$*, the matrices* A_{kj} *defined in* (16) *are stables,* $W_{\eta j}(\Delta u, X)$*,* $W_{\eta j}(\Delta u, \hat{X})$ *defined in* (16)*,* (17) *are equal to zero, and as* Ξ_{kj} *are positives definite, then the derivative of* V_{obs} (21) *reads*

$$\left\{\begin{array}{rcl}\dot{V}_{obs} & \leq & -\zeta_{1j}e_{1j}^T\Xi_{1j}e_{1j} \ldots - \zeta_{(p-1)j}e_{(p-1)j}^T\Xi_{(p-1)j}e_{(p-1)j} \\ & \leq & -\zeta V_{obs}\end{array}\right. \quad (26)$$

where $\zeta_j = min\{\zeta_{1j}, ..., \zeta_{(p-1)j}\}$ *and* $\zeta_{kj} > 0$*.*

Finally, from situations 1 and 2, the worst inequality of $\dot{V}_{obs}$ *is given by* (24)*. Thus, by choosing the observer* (17) *gains* (ζ_{kj}) *as stated in* (25)*, capacitor voltages estimates* $\hat{V}_{ckj}$ *of the DC source midpoint multi-cell multi-level three phase FCI converge exponentially to their real values* V_{ckj} *where the rate of convergence is fixed by* ζ_{kj}*. This ends the proof.*

5. Stability analysis of the "observer based control strategy"

As mentioned in the introduction, the use of physical sensors to measure the capacitor voltages is to be avoided (cost and failures increasing, reliability reducing, ...). Consequently for real implementation, the measured capacitor voltages V_{ckj} used by the proposed control strategy (10)-(11) are replaced by their estimates $\hat{V}_{ckj}$ given by the proposed observer (17) (software sensor), resulting in the new control strategy

$$\Delta u_{kj} = -sign(i_j)sign(\Delta\hat{V}_{ckj}) \quad (27)$$

where $\Delta\hat{V}_{ckj} = \hat{V}_{ckj} - V_{ckj-ref}$.

Theorem 5.1. *Consider system (6) where (17) is an associated high gain* (ζ) *observer of (16). Under the action of the proposed control strategy* (27)*, capacitor voltages* V_{ckj} *of the DC source midpoint multi-level three phase FCI converge asymptotically to their references* $V_{ckj-ref}$*.*

Proof 5.2. *Let be*

$$V_T = V_{ctrl} + V_{obs} = \sum_{k=1}^{p-1}\frac{1}{2}\Delta V_{ckj}^2 + \sum_{k=1}^{p-1}e_{kj}^T\Xi_{kj}e_{kj} \quad (28)$$

the candidate Lyapunov function whose dynamics along the trajectory of (17) *(where* (27) *is applied) is*

$$\begin{array}{rcl}\dot{V}_T & \leq & -\sum_{k=1}^{p-1}|\Delta\hat{V}_{ckj}|\frac{|i_j|}{C_{kj}} + \sum_{k=1}^{p-1}P_re_{kj}sign(\Delta\hat{V}_{ckj})\frac{|i_j|}{C_{kj}} \\ & & -\alpha_jV_{obs}\end{array}$$

where $V_{ckj-ref}$ *is considered constant and* $P_r = \begin{pmatrix}0 & 1\\ 0 & 0\end{pmatrix}$*. By selecting* ζ_{kj} *in* (25) *large enough, the dynamics of the observer will be fast, then* e_{kj} *will have a fast exponential convergence to zero (*$\hat{V}_{ckj}$ *will converge fast to* V_{ckj}*). Consequently*

$$\dot{V}_T \leq -\sum_{k=1}^{p-1}|\Delta V_{ckj}|\frac{|i_j|}{C_{kj}} - \gamma V_{obs}. \quad (29)$$

From (29)*, it can be concluded that capacitor voltages* V_{ckj} *of the DC source midpoint multi-cell multi-level three phase FCI track their reference trajectories* $V_{ckj-ref}$ *under the action of the proposed control strategy* (27)*. This ends the proof.*

6. Experimentation

In this section, the proposed control strategy associated with the designed observer in closed loop is implemented in case of a DC bus midpoint 3-cells 4-levels 3-phase FCI. In this case, p in (16) and (17) is replaced by 3, which gives $k = 1, 2$. Recall that j refers to legs a, b and c of the considered FCI. According to (25), the observer gains are chosen as follows: $\zeta_{1j} = \zeta_{2j}$=1000 (more details about the choice of these gains can be found in Ghanes et al. (2014)).

6.1. Test bench description

The experiment test bench is shown in Figure 2. It is composed of a 3-cells 4-levels three phase flying capacitor inverter fed by a continuous supply obtained with a bridge rectifier and connected to a RL load. To control it, two electronic boards from GS Maintenance company are used. The first board is the SCR_Flex that is based on a $TMS320F2812$ Texas Instruments DSP and a Spartan 3 Xilinx FPGA. Its function is to compute the proposed observer based direct control and generate the state switching vector for 3 legs (only a state of upper IGBTs). The same FPGA device is present in the second board which is named K_AMS. This board is used to generate the complementary signals for 3 legs (a state of lower IGBTs) with a configurable deadband time. The software deployed in the DSP is generated from Matlab/Simulink models and the VHDL language is used for programming the 2 FPGA devices. The behavior of this back is similar to the case of a dSPACE board, consequently, the experimental results in real time are obtained in Matlab window.
The inverter parameters are the following

- E = 300 V; $C_{1j} = C_{2j}$ = 470 μF;
- Switching frequency : f_s = 2 kHz;
- Sample period : 100 μs;
- L_j = 60 mH; R_j = 5 Ω.

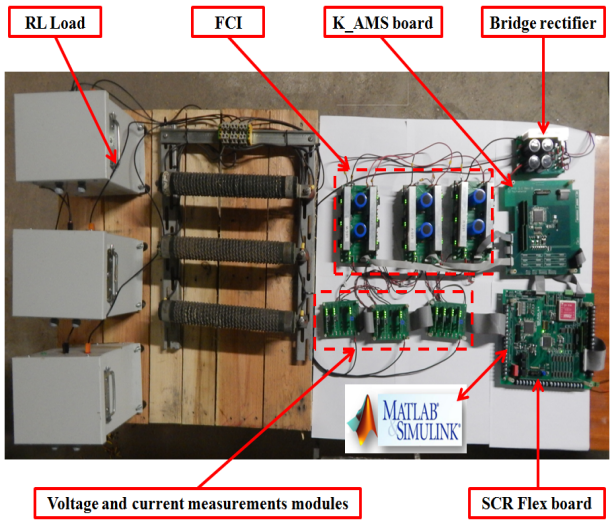

Figure 2: 3-cells 4-levels FCI test bench in GS Maintenance company.

Notice that the reference frequency of the inverter output is $f_{ref} = 50Hz$ for the three cells and $f_{ref} = 10Hz$ for the seven cells. Different output reference frequencies are chosen in order to show the influence of this frequency on the reference of the capacitor voltages.
In addition to this, it is important to highlight that the capacitor voltages measurements (real) are only given for comparison with their estimations.

6.2. Experimental results

Nominal test.
In this section, the results obtained from the proposed observer based control strategy are shown. The balanced load currents i_a, i_b and i_c are displayed in Figure 3. It can be observed that its have a same amplitude of 7.7 A and have a frequency of 50 Hz. The three phase output voltages of inverter is shown in Figure 4. It can be noted that its contain 4 levels: ±50 V and ±150 V as expected for the considered 3-cells inverter.

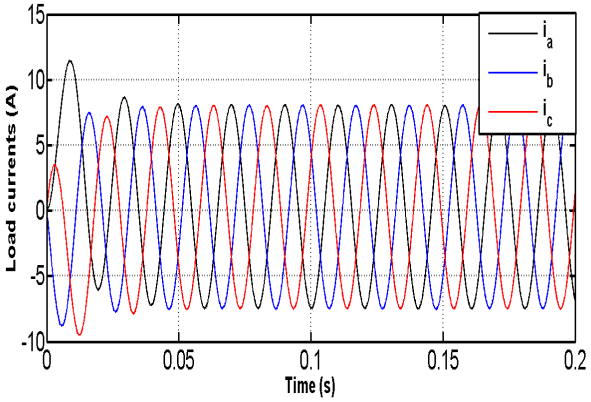

Figure 3: Load currents.

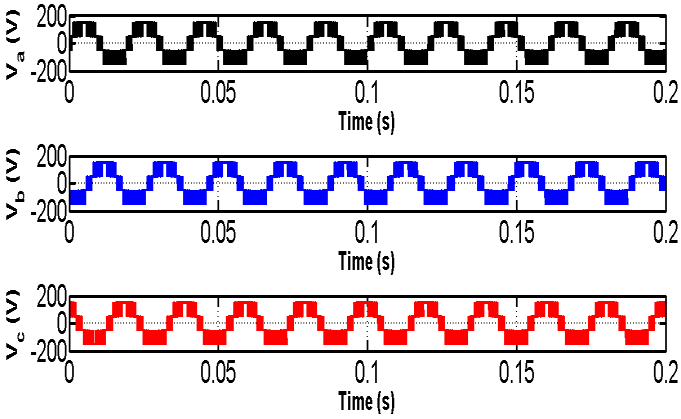

Figure 4: Output voltages.

In Figure 5a and Figure 5c, it can be remarked that capacitor voltages (real or measured) are well maintained around their references ($\frac{E}{3}$ and $\frac{2*E}{3}$ for V_{c1} and V_{c2}, respectively) by the proposed control strategy that uses in closed loop the capacitor voltages estimation. At the same time, the proposed observer follows the real capacitor voltages accurately.
Besides, in Figure 5b and Figure 5d, the errors between the real value and its reference converge and are still around 0, enhancing the performances of the observer based control.

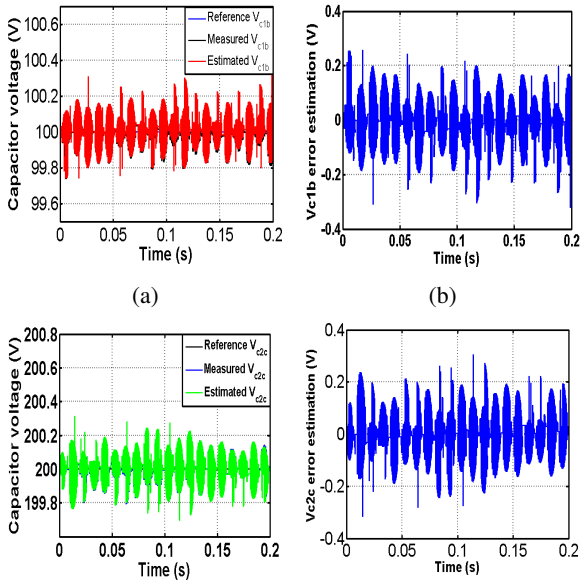

Figure 5: Floating capacitor voltages.
(a) $V_{c1b-ref}$, V_{c1b}, $\hat{V}_{c1b}$. (b) $\Delta V_{c1b} = V_{c1b} - V_{c1b-ref}$.
(c) $V_{c2c-ref}$, V_{c2c}, $\hat{V}_{c2c}$. (d) $\Delta V_{c2c} = V_{c2c} - V_{c2c-ref}$.

The transient state is showed by the 3-D representation in Figure 6 in which it is noticed that at start-up, the tracking error (between reference and measured voltages) and the estimation errors (between measured and estimated voltages) converge quickly to 0.

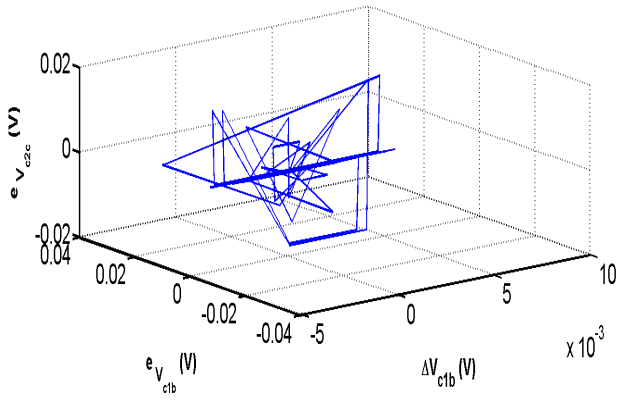

Figure 6: Floating capacitor voltages: tracking and estimation errors in three-dimensional representation.
$\Delta V_{c1b} = V_{c1b} - V_{c1b-ref}$.
$e_{V_{c1a}} = V_{c1b} - V_{c1b-ref}$.
$e_{V_{c6a}} = V_{c2c} - V_{c2c-ref}$.

Robustness tests.

To test the robustness of the proposed observer based control strategy, the DC bus voltage has been increased in the set-up from 300 V to 360 V at t=0.1 s (Figure 7). It can be remarked that real capacitor voltages V_{c1} and V_{c2} converge to the reference values in less than 0.01 s after the disturbance. Moreover the observer reacts quickly with a good accurate estimation of capacitor voltages used by the control strategy in closed-loop.

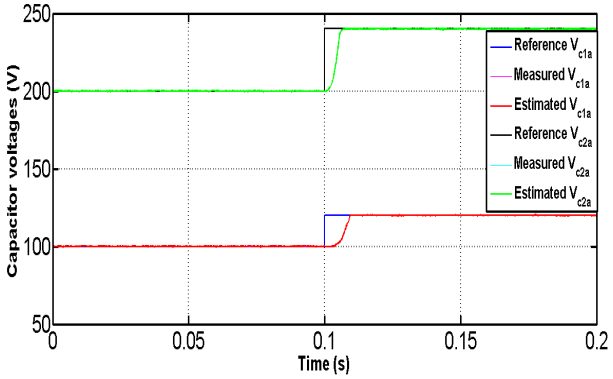

Figure 7: Floating capacitor voltages: $V_{c1a-ref}$, V_{c1a}, $\hat{V}_{c1a}$ and $V_{c2a-ref}$, V_{c2a}, $\hat{V}_{c2a}$ with DC bus variation.

Further, the effect of parameters variations is investigated by changing the cell capacitor C and the load resistance R parameters in the observer based control strategy within +50% of their nominal values. It is clear from results plotted in Figure 8a and Figure 8c that the tracking and estimation of capacitor voltages is well done and the effect of the capacitor cell C and the load resistance R variations is not remarkable.

This result is confirmed by Figure 8b and Figure 8d, which show that the error between the estimated voltage and the reference voltage is around 0.

This statement can be explained by the fact that the dedicated observer is robust against these variations. In fact, the correction term of the observer (which depends on the estimation error) is computed so that it is adapted to the variation of these parameters.

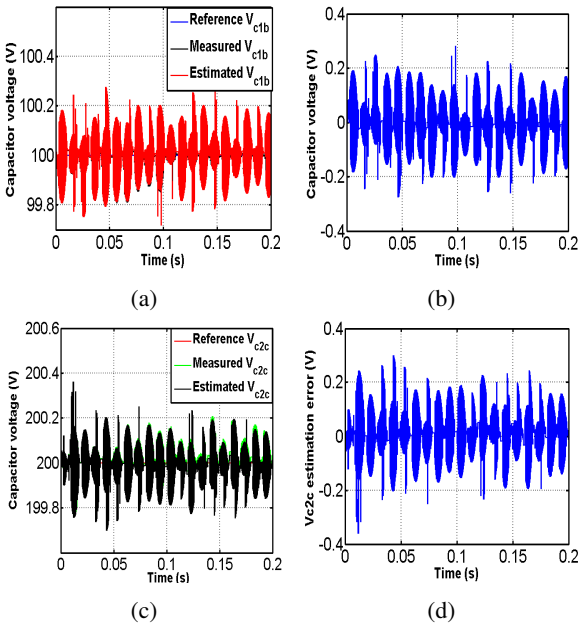

Figure 8: Floating capacitor voltages.
(a) $V_{c1b-ref}$, V_{c1b}, $\hat{V}_{c1b}$ with capacitor variation (+ 50%).
(b) $\Delta V_{c1b} = V_{c1b} - V_{c1b-ref}$ (+ 50% of C).
(c) $V_{c2c-ref}$, V_{c2c}, $\hat{V}_{c2c}$ with resistance variation (+ 50%).
(d) $\Delta V_{c2c} = V_{c2c} - V_{c2c-ref}$ (+ 50% of R).

Comparison with a PWM control.

Two PWM controls proposed in Khazraei et al. (2010) and Hemici et al. (2015) are compared to the proposed control strategy under transient and steady state operating modes. Each control is associated with the proposed observer in closed loop. The comparison is made in terms of time response and total harmonic distortion (THD) by using the same switching frequency ($f_s = 2kHz$) and the same power ($2kW$), for each control strategy. Note that in PWM control strategy, the control signal of each inverter power switches is generated by the intersection between carrying triangular signals delayed by $\frac{2\pi}{p}$ within frequency f_s and sinusoidal modulating signals within frequency f_{ref}. For each PWM control (Hemici et al. (2015), Khazraei et al. (2010)), the modulating signals are imposed by PI controllers output (duty cycles), which are applied to the average model (7) of each capacitor voltages. Then, PI gains are deduced as follows: $k_p = \frac{2\zeta 2\pi f_{PI} C}{i}$, $k_i = \frac{C(2\pi f_{PI})^2}{i}$.

In general, the bandwidth cutoff frequency of PI controllers (f_{PI}) could be much lower than the switching frequency. Here, a limit value of f_{PI} is chosen to have the largest PI bandwidth ($f_{PI} \leq \frac{f_s}{2} = 1kHz$). The damping coefficient ζ is set to $0,7$ and i is the nominal load current ($7.7A$).

The same test of a DC bus variation (variation from 300 V to 360 V at 0.1 s) is made as in Figure 7.

As can be seen in Figure 9, the proposed observer based control strategy reacts more quickly than the observer based PWM control in terms of the convergence of capacitor voltages to their references. For the proposed observer based control (Figure 9a), the response time is about $0.007\ s$, while in the observer based PWM controls 1 (Figure 9b) and 2 (Figure 9c), it is respectively $0.019\ s$ and $0.02\ s$.

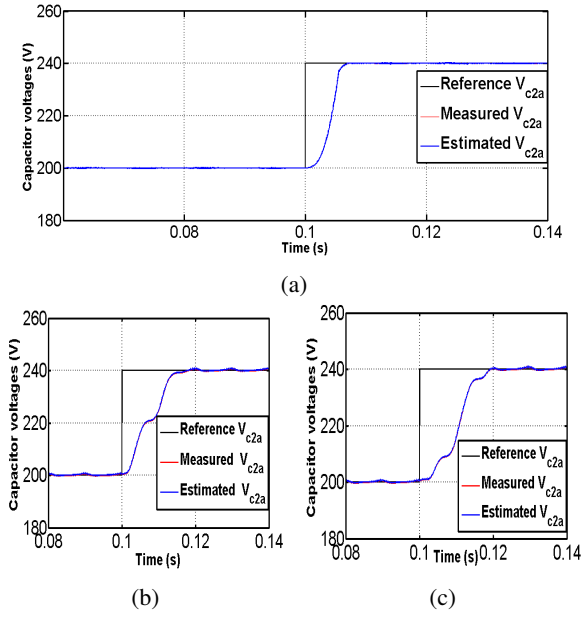

(a) (b) (c)

Figure 9: Floating capacitor voltages: $V_{c2a-ref}$, V_{c2a}, $\hat{V}_{c2a}$.
(a) Proposed observer based control.
(b) Observer based PWM control 1.
(c) Observer based PWM control 2.

Moreover, at steady state conditions, Figure 10 shows that the THD in the case of the proposed observer based direct control strategy (THD =35.9% in Figure 10a) is lower than the case when the observer is associated with a PWM control 1 (THD =37.96% in (Figure 10b)) or with PWM control 2 (THD =38.03% in (Figure 10c)).

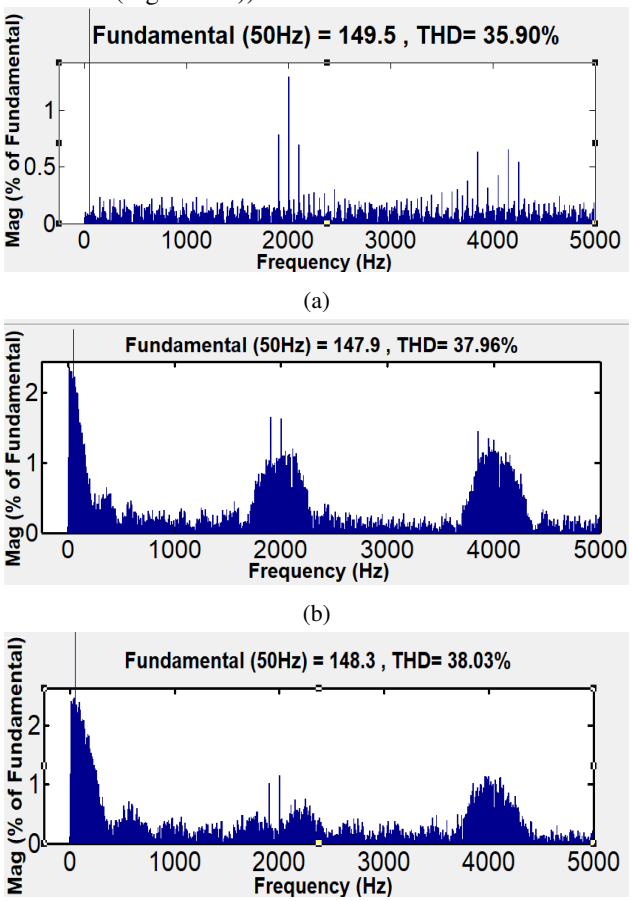

(a) (b) (c)

Figure 10: FFT harmonic spectrum of the output voltage V_b.
(a) Proposed observer based control.
(b) Observer based PWM control 1.
(c) Observer based PWM control 2.

Table 2 summarizes the comparison between the proposed control strategy and both PWM control laws.

criterion	Proposed	PWM 1	PWM 2
Power	2 kW	2 kW	2 kW
Response time	0.007 s	0.019 s	0.02 s
THD	35.9	37.96	38.03

Table 2: Comparison between the proposed observer based direct control and two observer based PWM controls.

6.3. Application to a 7-cells 8-levels FCI

To show that the proposed observer based control strategy is scalable for any number of cells, it was associated with a 7-cells 8-levels three phase FCI. This inverter has the same parameters described in section 6.1, except for E and f_{ref} that are equal to $308V$ and $10Hz$, respectively. Simulation results for

the observer based direct control of the 7-cells 8-levels FCI are presented in Figure 11. Thanks to the use of estimated voltages (computed by the proposed observer) in the direct control strategy, the real voltages reach and are maintained around their references, respectively $\frac{E}{7} = 44V$ and $6\frac{E}{7} = 264V$ for V_{c1a} and V_{c6b}. It can be remarked that the estimated voltages track the real values perfectly. The three phase output voltages of inverter are presented in Figure 11e. It can be remarked that it contains 8 levels: ±22 V, ±66 V, ±110 V and ±154 V as expected for the considered 7-cells inverter.

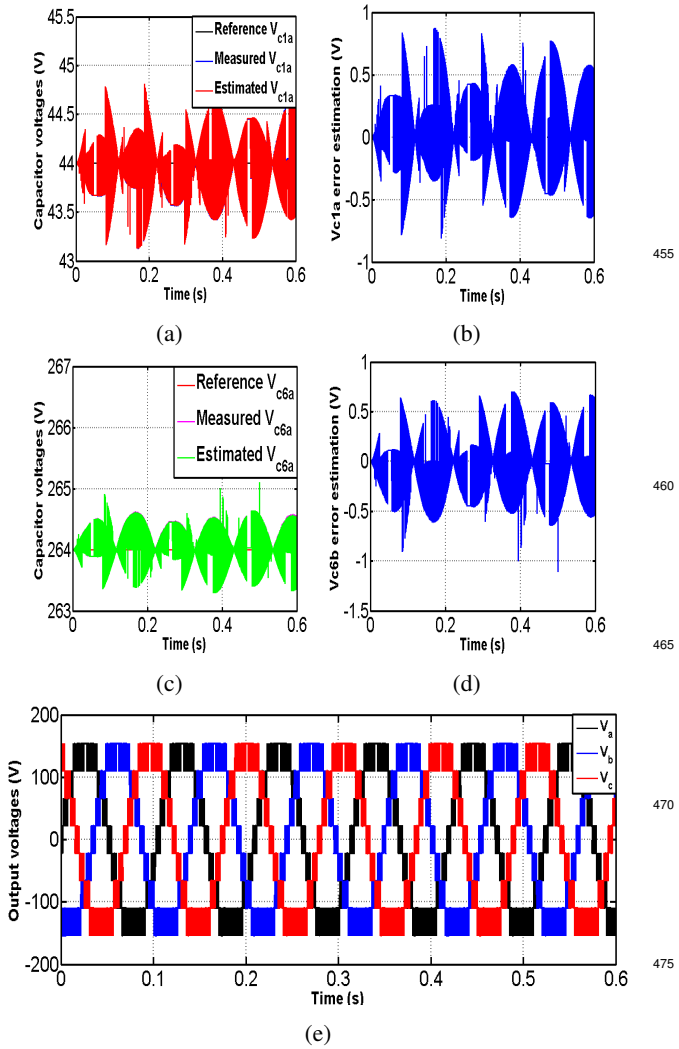

Figure 11: Simulation results in case of a 7-cells 8-levels FCI.
(a) $V_{c1a-ref}$, V_{c1a}, $\hat{V}_{c1a}$.
(b) $\Delta V_{c1a} = V_{c1a} - V_{c1a-ref}$.
(c) $V_{c6b-ref}$, V_{c6b}, $\hat{V}_{c6b}$.
(d) $\Delta V_{c6b} = V_{c6b} - V_{c6b-ref}$.
(e) Output voltages.

The 3-D representation in Figure 12 shows the response of the proposed observer based control strategy in start-up conditions. It can be concluded, that the observer based direct control is characterized by a fast dynamic performance in tracking the reference values of capacitor voltages.

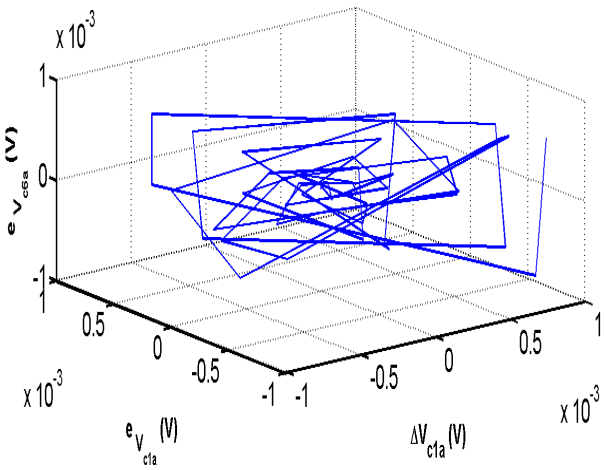

Figure 12: Tracking and estimation errors in three-dimensional representation for a 7-cells 8-levels FCI. $\Delta V_{c1a} = V_{c1a} - V_{c1a-ref}$.
$e_{V_{c1a}} = V_{c1a} - V_{c1a-ref}$.
$e_{V_{c6a}} = V_{c6a} - V_{c6a-ref}$.

7. Conclusion

In the first contribution of this work, the control strategy (Laamiri et al. (2017)) that combines the projection strategy with a classical sliding mode technique, is generalized for a DC bus midpoint three-phase FCI with any number of cells. The control strategy that allows to achieve the tracking of capacitor voltages to their references, uses voltage sensors which are expensive and cumbersome because of the high voltages and the increase of the number of cells. Moreover, the reliability of the inverter is reduced because sensors can fail. Thus, the advantage of suppressing a sensor voltages and using an observation technique becomes evident. From this point of view, the second contribution of this work was to propose an adaptive observer to estimate the capacitor voltages for a DC bus midpoint three-phase FCI with any number of cells. Moreover, the stability of the proposed observer based direct control strategy for a multi-cell three-phase FCI scalable to any number of cells is proved by means of Lyapunov theory. Experimental results in the case of a 3-cells 4-levels three-phase FCI showed that the proposed direct control in closed-loop with estimated voltages offers a good performance in tracking the reference values and insures the robustness against the input variation, cell capacitor variation and load resistance variation. Then, a better quality of the output voltage is obtained compared to the association of the proposed observer with a PWM control. The proposed observer based control strategy is applied to the case of a 7-cells 8-levels three-phase FCI. The obtained simulation results are satisfactory and allow to highlight the applicability of the proposed strategy for any FCI number of cells. Tests of the observer based direct control strategy for this type of inverter (7-cells 8-levels three-phase FCI) in a real-time set-up is the perspective of this work. This set-up is in progress and it is considered as confidential at GS Maintenance company.

References

Aguilera, R.P., Lezana, P., Quevedo, D.E., 2015. Switched model predictive control for improved transient and steady-state performance. IEEE Transactions on Industrial Informatics 11, 968–977.

Al-Hammouri, A.T., Nordström, L., Chenine, M., Vanfretti, L., Honeth, N., Leelaruji, R., 2012. Virtualization of synchronized phasor measurement units within real-time simulators for smart grid applications, in: 2012 IEEE Power and Energy Society General Meeting, pp. 1–7.

Ben Said, S., Ben Saad, K., Benrejeb, M., 2014. On two control strategies for multicellular converters. International Journal of control, Energy and Electrical Engineering (CEEE) 1, 37–42.

Benzineb, O., Taibi, F., Benbouzid, M., Boucherit, M., Tadjine, M., 2011. Multicell converters hybrid sliding mode control. International Review on Modelling and Simulations 4, 1396–1403.

Benzineb, O., Taibi, F., Laleg-Kirati, T.M., Boucherit, M., Tadjine, M., 2013. Control and fault diagnosis based sliding mode observer of a multicellular converter: Hybrid approach. Journal of Electrical Engineering 64, 20–30.

Brychcín, J., Janik, D., Kosan, T., Peroutka, Z., 2016. Modulator for 4-level flying capacitor converter with balancing control in the closed loop. Transactions on Electrical Engineering 5, 66–69.

Béthoux, O., Barbot, J.P., Hilairet, M., 2008. Multicell actuator based on a sliding mode control. The European Physical Journal Applied Physics 43, 217–223.

Defoort, M., Djemai, M., Floquet, T., Perruquetti, W., 2011. Robust finite time observer design for multicellular converters. International Journal of Systems Science 42, 1859–1868.

Eriksson, K., Jonsson, T., Tollerz, O., 1998. Small scale transmission to ac networks by hvdc light, in: 12th Cepsi conference, Thailand.

Ghanes, M., Trabelsi, M., Abu-Rub, H., Ben-Brahim, L., 2016. Robust adaptive observer-based model predictive control for multilevel flying capacitors inverter. IEEE Transactions on Industrial Electronics 63, 7876–7886.

Ghanes, M., Trabelsi, M., lin shi, X., Barbot, J.P., Retif, J., Busawon, K., 2014. High gain observer for a three-cell chopper: Design and experimental results. International Journal of Robust and Nonlinear Control 24, 1090–1103.

Hemici, K., Zegaoui, A., Bokhtache, A.A., Mahmoudi, M., Aillerie, M., 2015. Three-phases flying-capacitor multilevel inverter with proportional natural pwm control. Energy Procedia 74, 1061 – 1070.

Hosseini, S.H., Sadig, A.K., Sharifi, A., 2009. Estimation of flying capacitors voltages in multicell converters, in: 2009 6th International Conference on Electrical Engineering/Electronics, Computer, Telecommunications and Information Technology, pp. 110–113.

Kang, W., Barbot, J.P., Xu, L., 2009. On the observability of nonlinear and switched systems, in: Ghosh, B.K., Martin, C.F., Zhou, Y. (Eds.), Emergent Problems in Nonlinear Systems and Control.

Khazraei, M., Sepahvand, H., Corzine, K., Ferdowsi, M., 2010. A generalized capacitor voltage balancing scheme for flying capacitor multilevel converters, in: 2010 Twenty-Fifth Annual IEEE Applied Power Electronics Conference and Exposition (APEC), Palm Springs, CA, USA. pp. 58–62.

Laamiri, S., Ghanes, M., Amet, L., Santomenna, G., 2017. Direct control strategy for a three phase eight-level flying-capacitor inverter, in: 20th IFAC World Congress.

Lezana, P., Rodriguez, J., Oyarzun, D.A., 2008. Cascaded multilevel inverter with regeneration capability and reduced number of switches. IEEE Transactions on Industrial Electronics 55, 1059–1066.

Lygeros, J., Johansson, K.H., Simic, S.N., , Sastry, S.S., 2003. Dynamical properties of hybrid automata. IEEE Transactions on Automatic Control 48, 2–17.

Meynard, T.A., Foch, H., 1992. Dispositif de conversion d'énergie électrique à semiconducteur. Brevet français 00652, 09582.

Meynard, T.A., Foch, H., Forest, F., Turpin, C., Richardeau, F., Delmas, L., Gateau, G., Lefeuvre, E., 2002. Multicell converters: derived topologies. IEEE Transactions on Industrial Electronics 49, 978–987.

Poznyak, A., Polyakov, A., Strygin, V., 2011. Analysis of finite-time convergence by the method of lyapunov functions in systems with second-order sliding modes. Journal of Applied Mathematics and Mechanics 75, 289 – 303.

Sadigh, A.K., Hosseini, S.H., Sabahi, M., Gharehpetian, G.B., 2010. Double flying capacitor multicell converter based on modified phase-shifted pulsewidth modulation. IEEE Transactions on Power Electronics 25, 1517–1526.

Shukla, A., Ghosh, A., Joshi, A., 2011. Natural balancing of flying capacitor voltages in multicell inverter under pd carrier-based pwm. IEEE Transactions on Power Electronics 26, 1682–1693.

Stala, R., Pirog, S., Baszynski, M., Mondzik, A., Penczek, A., Czekonski, J., Gasiorek, S., 2009. Results of investigation of multicell converters with balancing circuit—part i. IEEE Transactions on Industrial Electronics 56, 2610–2619.

Thielemans, S., Ruderman, A., Reznikov, B., Melkebeek, J., 2010. Simple time domain analysis of a 4-level h-bridge flying capacitor converter voltage balancing, in: 2010 IEEE International Conference on Industrial Technology (ICIT 2010), pp. 818–823.

Van Nguyen, T., Jeannin, P., Vagnon, E., Frey, D., Crebier, J., 2010. Series connection of igbt, in: 2010 Twenty-Fifth Annual IEEE Applied Power Electronics Conference and Exposition (APEC), pp. 2238–2244.